

Supporting Information

Surface Charges Self-Recovery Electret Film against Harsh Environment for Wearable Energy Conversion

Junwen Zhong^{1†}, Qize Zhong^{1†}, Gangjin Chen², Bin Hu¹, Sheng Zhao¹, Xin Li¹, Nan Wu¹,

Wenbo Li¹, Huimin Yu¹, Jun Zhou^{1}*

¹Wuhan National Laboratory for Optoelectronics, School of Optical and Electronic Information, Huazhong University of Science and Technology, Wuhan, 430074, China

²Laboratory of Electret and Its Application, Hangzhou Dianzi University, Hangzhou, 310018, China

[†]These people contributed equally to this work.

*Correspondence to: jun.zhou@mail.hust.edu.cn

Supplementary Note 1: Power generating mechanism analysis based on a finite element simulation.

The variation of electric potential distribution and charges transfer between the top and bottom electrodes during the power generation process of the sandwich-structured flexible electret generator are ideally evaluated by a finite element simulation (COMSOL Multiphysics software). In the generator, the variation of electric potential distribution mainly depends on the two air gap distances between the laminated EVA/BOPP cellular electret film and two electrodes. In the original state, the electric potential distribution of the two electrodes is in equilibrium state and no charges will transfer (**Figure S7a**). When the generator is pressed, more positive and negative charges will be induced in the top and bottom electrode, respectively, as the two air gap distances become smaller. Therefore, the electric potential equilibrium state is broken and positive charges will flow from bottom electrode to top electrode to reach the new equilibrium state. When the generator is released, the variation of electric potential distribution and charge transfer are opposite to the pressing process. The pressing and releasing process will generate a positive and negative current signal, respectively, if the positive pole of the ampere meter is linked to the bottom electrode (**Figure S7b**). Switching polarity test is also carried out to confirm that the measured output signals are not generated from the measurement system (**Figure 7b**).

The open-circuit voltage and transferred charges dependence of the air gap distance can be calculated according to above ideal model. The open-circuit voltage varies linearly as the air gap distance getting smaller gradually, from ~ 0 V in ~ 300 μm to ~ 600 V in ~ 0 μm (**Figure S7c**). However, nearly 70 % of charges transfer is finished when the air gap becomes smaller than 100 μm (**Figure S7d**).

Supplementary Note 2: Electrical output performances of the sandwich-structured flexible generator

The electrical output performances of the generators were carefully studied by periodically pressing and releasing at controlled frequencies and forces provided by a resonator. Typically, the generators were attached to a force meter, which was tightly fixed onto an x-y-z mechanical stage.

Figure S8a and **Figure S8b** indicate the output currents and corresponding transferred charges (ΔQ) under the same conditions (5 Hz, 5 N, 20 M Ω) for 3 flexible electret generators with laminated cellular electret film as the electrostatic field source. The 3 flexible electret generators are sandwich-structured flexible electret generator, arch-structured flexible electret generators with aluminum (Al) electrode on BOPP and EVA side of the laminated cellular electret film, respectively. The output performances of the sandwich-structured flexible generator were obviously more excellent than that of the arch-structured flexible electret generators, since the sandwich-structured generator can adequately utilize electrostatic induction caused by negative and positive charges on EVA and BOPP side.

The Output currents and corresponding ΔQ under the same conditions (5 Hz, 5 N, 20 M Ω) for 3 flexible electret generators with the same structure but with different electret materials are indicated in **Figure S8c** and **Figure S8d**. Specifically, the output performances for the sandwich-structured flexible generator with laminated cellular electret film as electret material were significantly better than that of the devices with BOPP or EVA film as electret materials, which demonstrates the outstanding surplus charges capturing ability of the laminated cellular electret film.

Figure S8e indicates the load peak currents and corresponding ΔQ for the sandwich-structured flexible generator under different stimulated force and a given stimulated frequency of 5 Hz. The load peak currents increased approximately linearly, when the

stimulated force was less than 1 N. With the stimulated force getting larger than 1 N, the increasing rate of the load peak currents became less. The variation tendency of the ΔQ was similar to that of the load peak currents, which were divided to two regions. Besides, for a given stimulated force of 5 N and increasing stimulated frequencies, the load peak currents increased step by step, but the ΔQ almost kept at a constant value (**Figure S8f**). The load peak currents of the sandwich-structured flexible generator are related to both stimulated frequency and force, and the ΔQ is only related to stimulated force.

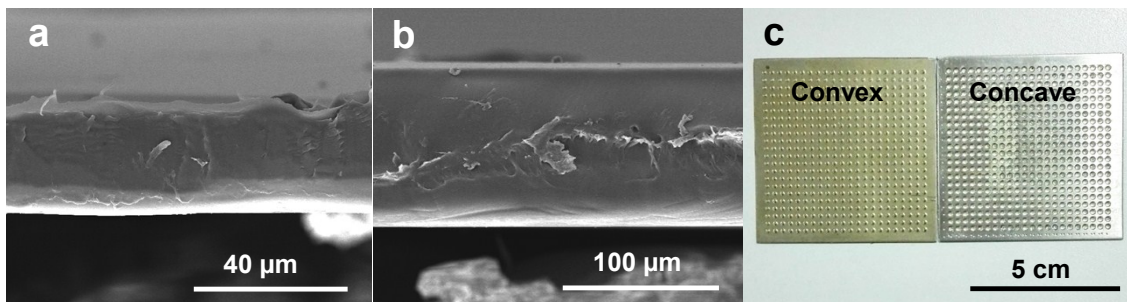


Figure S1. Cross section view SEM images for (a) BOPP and (b) EVA raw films, respectively. (c) Digital picture for convex and concave stainless steel masks with regular patterns.

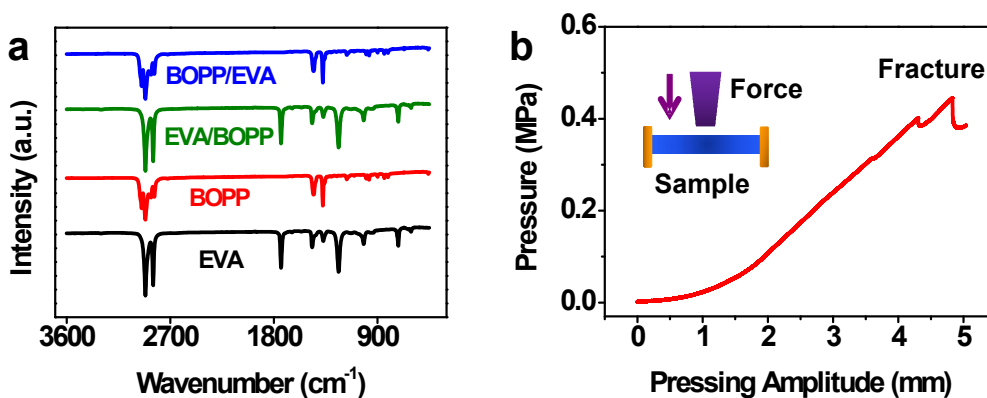


Figure S2. (a) FTIR spectrums for EVA and BOPP film before and after fabrication process. (b) Fracturing performance for the laminated EVA/BOPP cellular electret film. Insert in (b) shows the schematic diagram for the measurement.

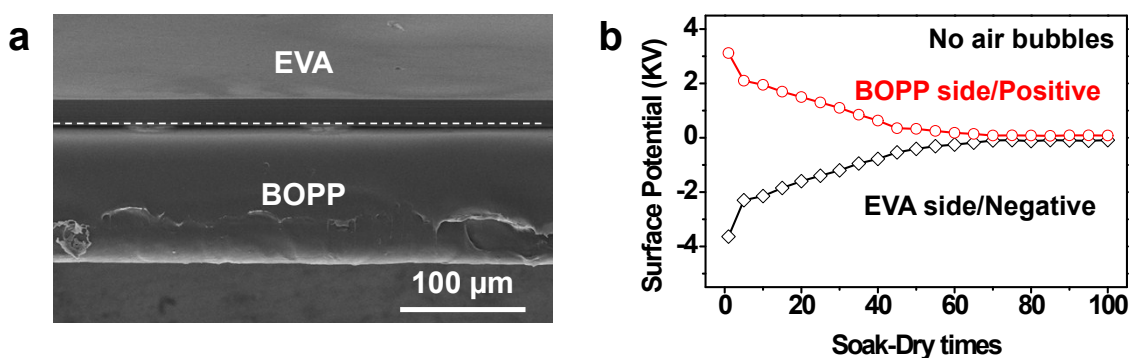


Figure S3. (a) Cross section view SEM image for laminated EVA/BOPP electret film without air bubbles. (b) Surface potential decay for this type of laminated electret film during continuous 100 soak-dry times.

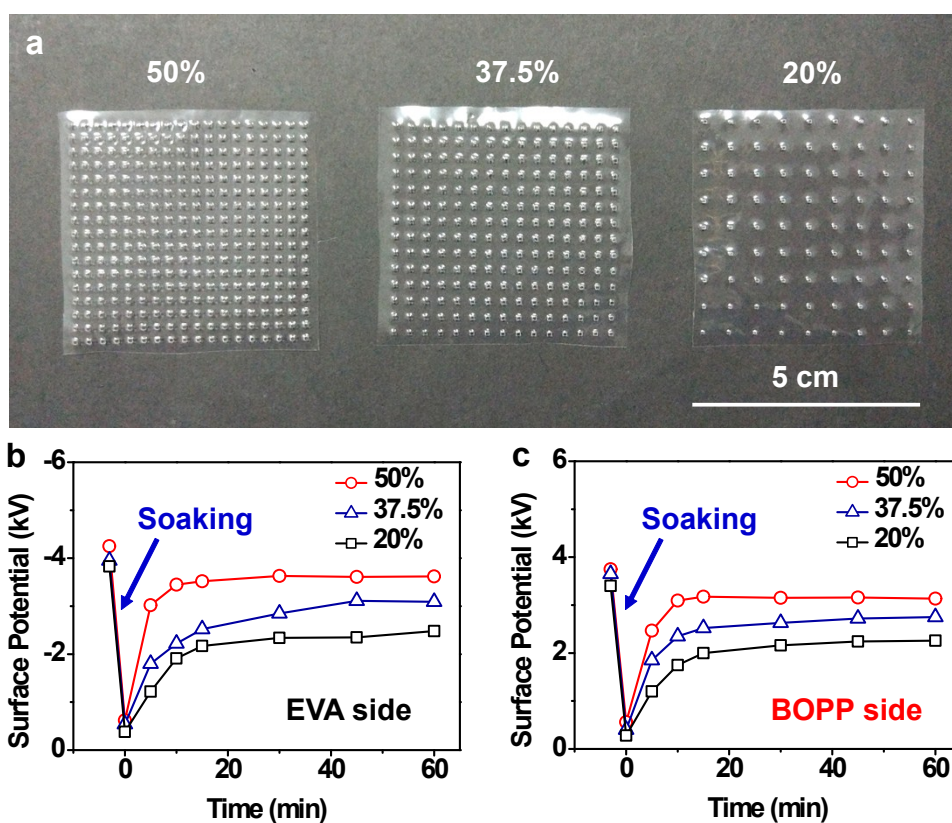


Figure S4. (a) Digital picture for laminated cellular electret films with ~ 20%, ~ 35% and ~ 50% area ratio. Surface potential self-recovery properties on (b) EVA side and (c) BOPP side for laminated cellular electret films with 20%, 35% and 50% area ratio, respectively.

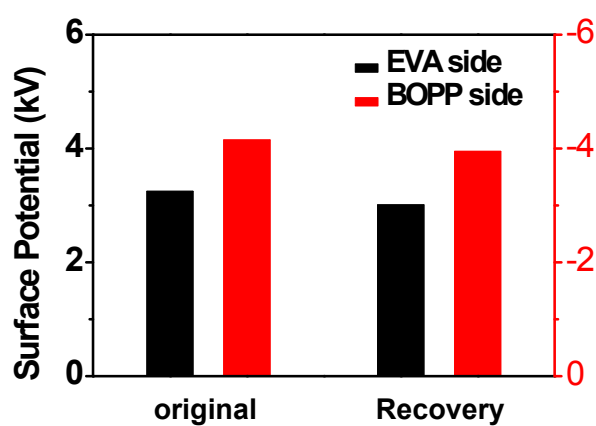


Figure S5. Surface potential self-recovery property for the laminated EVA/BOPP cellular electret film with BOPP side facing to the corona needle tip during negative corona charging.

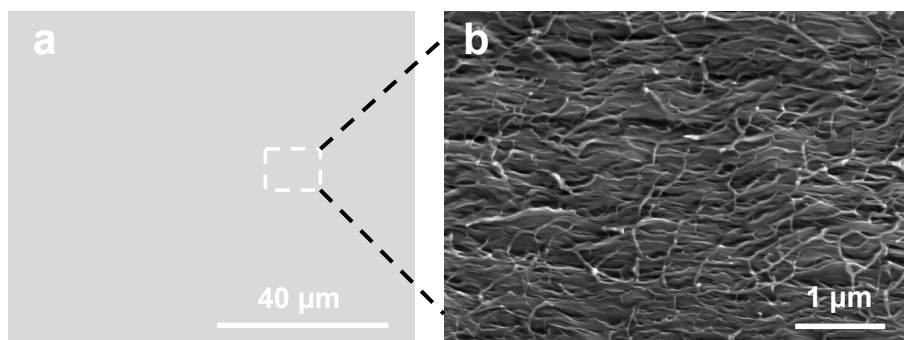


Figure S6. Low-magnification (a) and high-magnification (b) cross-section view SEM images for the BOPP raw film, respectively. Space charges will be captured in the nanoscale porous structure during corona charging process.

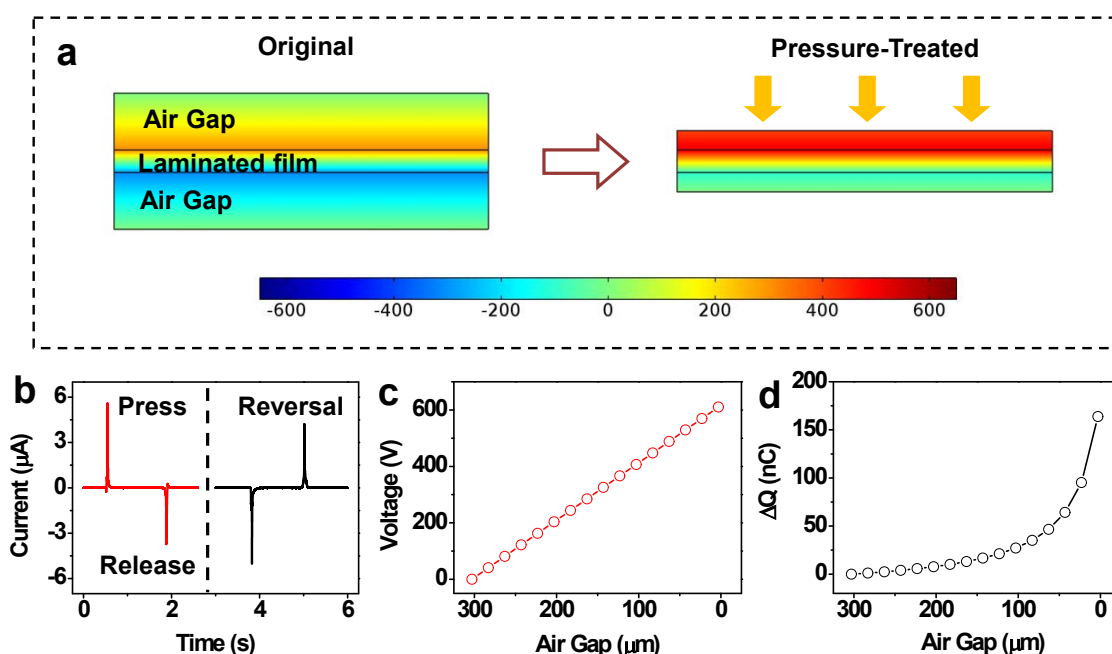


Figure S7. (a) The finite element simulation (COMSOL Multiphysics software) of the working mechanism for the sandwich-structured flexible electret generator, indicating the variation of electric potential distribution between the top and bottom electrodes under original and pressing state. (b) Current signals for hand pressing and releasing the generator with load resistance of 20 M Ω . Current signals for reverse-connecting to the ampere meter are also provided in (b). (c) Open-circuit voltage and (d) transferred charges (ΔQ)

dependence of the air gap distance calculated by COMSOL simulation.

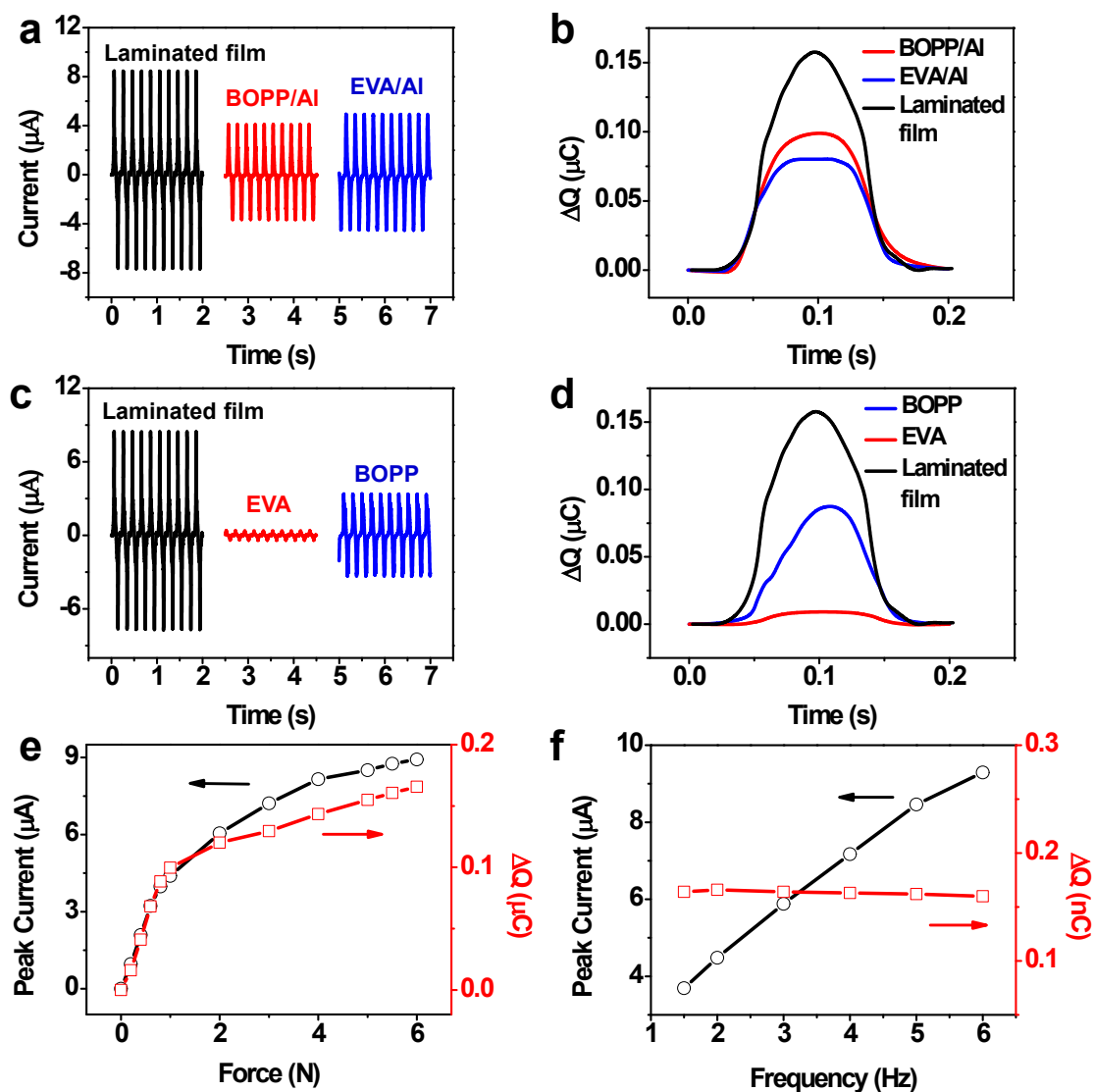


Figure S8. (a) Output currents and (b) corresponding transferred charges (ΔQ) under the same conditions (5 Hz, 5 N, 20 M Ω) for 3 flexible electret generators, which were our sandwich-structured flexible electret generator, arch-structured flexible electret generators with aluminum (Al) electrode on BOPP and EVA side of the laminated cellular electret film, respectively. (c) Output currents and (d) corresponding ΔQ under the same conditions (5 Hz, 5 N, 20 M Ω) for 3 flexible electret generators with different electret materials, which were laminated cellular electret film, EVA and BOPP raw films, respectively. Load peak currents and corresponding ΔQ for the sandwich-structured flexible electret generator (e) under a given stimulating frequency of 5 Hz and (f) a given stimulating force of 5 N, the load resistance was 20 M Ω .

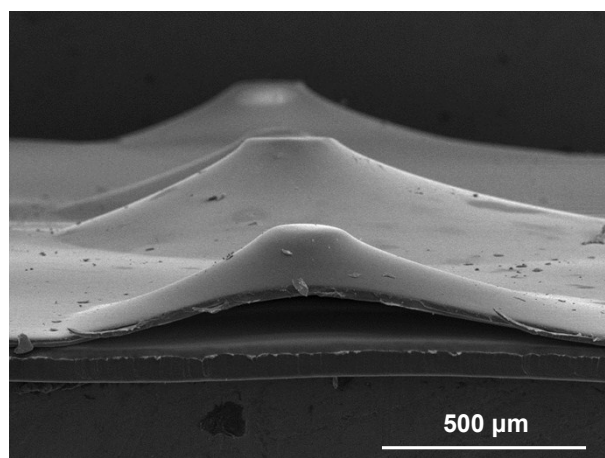


Figure S9. Cross-section view SEM image of the laminated cellular electret film after stability measurement.

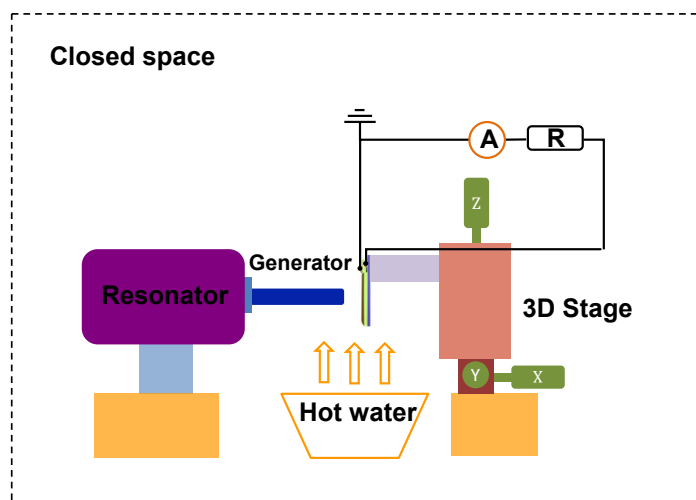


Figure S10. Electrical measurement system for generators placed in extreme moisture environment, which was provided by water vapor.

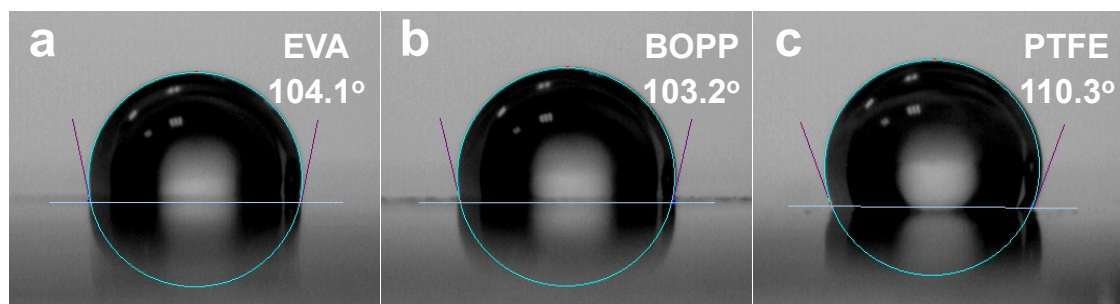


Figure S11. Contact angles for (a) EVA, (b) BOPP and (c) PTFE films, respectively, indicating that these materials can fully contacted with water vapor during the vapor-treating process.

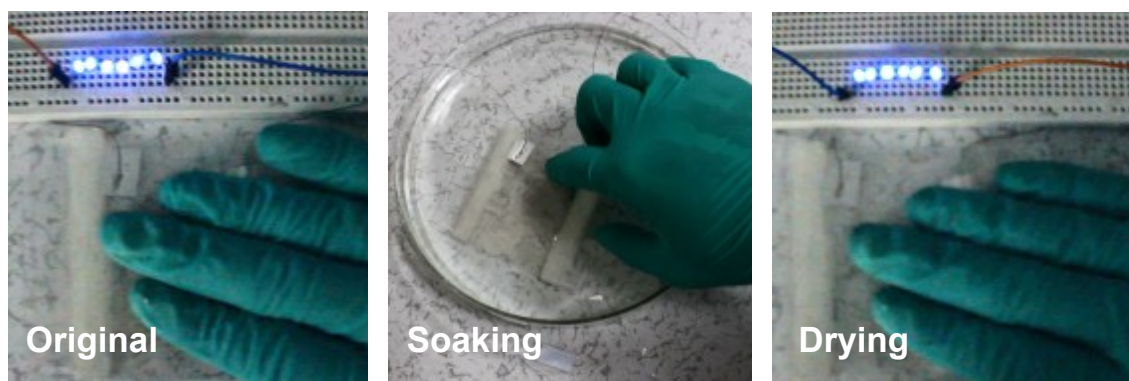


Figure S12. Six blue LDEs lit up by hand pressing the same sandwich-structured flexible electret generator before and after soaking in water.

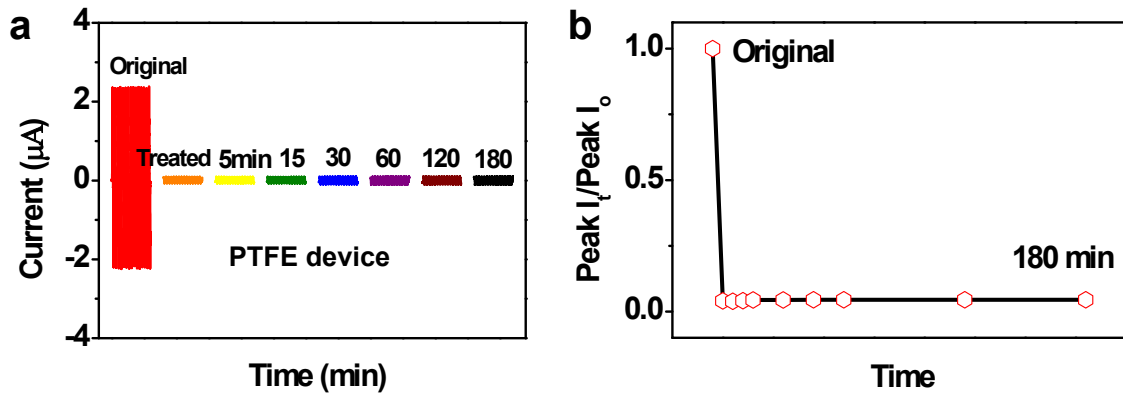


Figure S13. (a) Currents for the arch-structured PTFE flexible electret generator under vapor-treating process, under the 5 N force with 5 Hz frequency stimulating and load resistance of 20 M Ω . (b) Relative load peak current value for the generator under vapor-treating process.

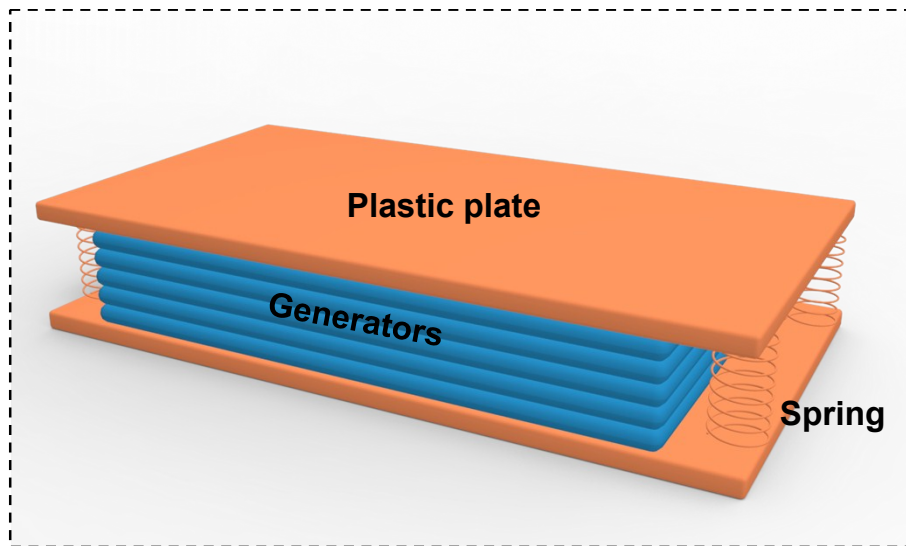


Figure S14. Schematic diagram for a power unit.

Supplementary Video 1: Lighting up 6 blue LDEs by hand pressing the same sandwich-structured flexible electret generator before and after soaking in water.

Supplementary Video 2: Working processes for the self-powered and self-triggered wireless emitting system.

Supplementary Video 3: Generators can autonomously power the wireless emitter with an effectively emitting distance of ~ 18 meters.